Acta Crystallographica Section D
Biological Crystallography
ISSN 0907-4449

The 1.5 Å structure of endo-1,3-β-glucanase from *Streptomyces sioyaensis*: evolution of the active-site structure for 1,3-β-glucan-binding specificity and hydrolysis

Tang-Yao Hong,[a]‡ Yu-Yuan Hsiao,[b]‡§ Menghsiao Meng[c] and TienHsiung Thomas Li[b]*

[a]Department of Biotechnology, Tajen University, Pingtung 907, Taiwan, [b]Institute of Biochemistry, National ChungHsing University, Taichung 40227, Taiwan, and [c]Graduate Institute Biotechnology, National ChungHsing University, Taichung 40227, Taiwan

‡ These authors contributed equally to this work.
§ Current address: Institute of Molecular Biology, Academia Sinica, Taipei 11529, Taiwan.

Correspondence e-mail: lithomas@dragon.nchu.edu.tw

Received 22 June 2008
Accepted 11 July 2008

PDB Reference: endo-1,3-β-glucanase catalytic domain, 3dgt, r3dgtsf.

The catalytic domain structure of *Streptomyces sioyaensis* 1,3-β-glucanase (278 amino acids), a member of glycosyl hydrolase family 16 (GHF16), was determined to 1.5 Å resolution in space group $P2_12_12_1$. The enzyme specifically hydrolyzes the glycosidic bond of the 1,3-β-linked glucan substrate. The overall structure contains two antiparallel six- and seven-stranded β-sheets stacked in a β-sandwich jelly-roll motif similar to the fold of GHF16 1,3–1,4-β-glucanases. The active-site cleft of the enzyme is distinct, with the closure of one end primarily caused by two protruding loop insertions and two key residues, Tyr38 and Tyr134. The current known structures of 1,3–1,4-β-glucanases and 1,3-β-glucanase from *Nocardiopsis* sp., on the other hand, have open-channel active-site clefts that can accommodate six β-D-glucopyranosyl units. The active-site structure of 1,3-β-glucanase was compared with those of other homologous structures in order to address the binding and enzymatic specificity for 1,3-β-linked glucans in *Streptomyces*. This information could be helpful in the development of specific antifungal agents.

1. Introduction

The 1,3-β-glucanases (EC 3.2.1.39), which are classified as members of glycosyl hydrolase family 16, hydrolyze the internal 1,3-β-D-glucosidic linkages in 1,3-β-D-glucans, which are major components of fungi and plant cell walls and the structural and storage polysaccharides (laminarin) of marine macro-algae. Hundreds of 1,3-β-glucanases have been isolated and characterized from plants, insects, fungi, bacteria and viruses (Selitrennikoff, 2001). Owing to their ability to hydrolyze 1,3-β-glucan, 1,3-β-glucanases are generally found to be involved in plant host self-defence against pathogenic invasion (Grenier *et al.*, 1993; Yi & Hwang, 1997) and bacterial inhibition of fungal growth (Watanabe *et al.*, 1992). Other functions of 1,3-β-glucanases, such as cell expansion, cell–cell fusion and spore release, have also been found in fungi (de la Cruz *et al.*, 1995). Despite their similar enzymatic activities, the enzymes from plants and bacteria share no similarities in amino-acid sequence: the plant 1,3-β-glucanases are classified into glycosyl hydrolase family 17 (GHF 17), while those from bacteria are grouped into GHF 16 (Henrissat, 1991). The bacterial 1,3-β-glucanases share sequence similarities to 1,3–1,4-β-glucanases (Gueguen *et al.*, 1997), which specifically hydrolyze 1,4-β-glucosidic bonds of β-glucans containing mixed 1,3-β- and 1,4-β-linkages. The recently published crystal

structure of a 1,3-β-glucanase (BglF) from the alkaliphile *Nocardiopsis* sp. strain F96 revealed a β-sandwich jelly-roll folding motif (Fibriansah *et al.*, 2007). The overall active-site structure is also similar to the known structures of 1,3–1,4-β-glucanases (GHF 16) from two *Bacillus* strains, *B. macerans* and *B. licheniformis* (Hahn, Olsen *et al.*, 1995; Hahn, Pons *et al.*, 1995), and of a 1,3–1,4-β-glucanase from *Fibrobacter succinogenes*, the C-terminal sequence of which is similar to the N-terminal sequences of other members of GHF16 (Tsai *et al.*, 2003).

Streptomyces sioyaensis exhibits antifungal activity against several fungal pathogens such as *Pythium aphanidermatum*, *Colletotrichum higginsianum*, *Acremonium lactucum* and *Fusarium oxysporum* (Chen *et al.*, 2000). The 478-amino-acid 1,3-β-glucanase from *S. sioyaensis* (NCBI GenBank accession No. AF217415) contains two functional domains linked by a flexible peptide of nine glycine residues. The N-terminal domain possesses enzymatic activity characteristic of bacterial endo-1,3-β-glucanases, while the C-terminal domain is a carbohydrate-binding module (CBM) belonging to CBM family 6 that enhances the activity of the catalytic domain toward insoluble 1,3-β-glucans. A substrate-binding assay indicated that the catalytic domain of the 1,3-β-glucanase preferentially catalyses the endolytic hydrolysis of glucans with 1,3-β-linkages, such as water-soluble laminarin and water-insoluble curdlan and pachyman [1,3-β-(glucose)] but not soluble lichenan [1,3–1,4-β-(glucose)]. BglF has more than eightfold greater activity toward 1,3–1,4-β-glucan at 333 K than the 1,3-β-glucanase from *Streptomyces*, which has low enzymatic activity toward 1,3–1,4-β-linked glucans (Hong *et al.*, 2002). Furthermore, the 1,3-β-glucanases from plants, such as barley and banana, share no primary or tertiary structural homology with the bacterial enzymes (Receveur-Brechot *et al.*, 2006; Varghese *et al.*, 1994). Here, we report the crystal structure of 1,3-β-glucanase from an *S. sioyaensis* strain at 1.5 Å resolution in order to study its substrate-binding specificity and enzymatic hydrolysis toward 1,3-β-glucans.

2. Materials and methods

2.1. Expression and purification

The procedure described by Hong *et al.* (2002) was used with slight modifications to purify the protein expressed in the *Escherichia coli* periplasm. The gene encoding the 1,3-β-glucanase catalytic domain, including the secretion-signal sequence at the 5′-end, was inserted between the *Hin*dIII and *Eco*RI sites of the pUC18 vector. The amino-acid sequence at the C-terminus of the expressed protein has a stretch of seven amino acids (–TSLSPGL) that differs from the sequence of the wild-type protein (–VLQSS). A 6 ml aliquot of an overnight culture of *E. coli* Tuner (DE3) cells (Novagen) containing the pUC18 vector was inoculated into 800 ml LB medium containing ampicillin (150 µg ml^{-1}). IPTG was added to a final concentration of 1.0 m*M* at an OD_{595} of ∼0.8. After induction of protein expression, the cell culture was shaken at 250 rev min^{-1} at 302 K for an additional 12 h. Cells were harvested by centrifugation, washed with buffer *A* (10 m*M* Tris–HCl pH 7.0, 30 m*M* NaCl), resuspended in 40 ml buffer *B* (30 m*M* Tris–HCl pH 7.0) and then mixed with an equal amount of hypertonic buffer [30 m*M* Tris–HCl pH 7.0, 40%(*w*/*v*) sucrose, 0.2 m*M* EDTA] for 20 min at 277 K. The *E. coli* periplasmic proteins were then extracted by replacing the buffer with 0.5 m*M* $MgCl_2$. The protein solution was mixed with an equal amount of 10 m*M* sodium acetate pH 4.0, stirred for 20 min and centrifuged; the clear supernatant was then collected. The solution containing the qualitatively purified periplasmic proteins was applied onto a HiTrap SP column (Pharmacia) pre-equilibrated with 10 m*M* sodium acetate pH 4.0. The 1,3-β-glucanase activity passed directly through the column. The sodium acetate enzyme solution buffer was then exchanged for 10 m*M* potassium phosphate buffer pH 8.0 and the solution was applied onto a HiTrap Q column (Pharmacia) pre-equilibrated with 10 m*M* sodium acetate pH 4.0 and the flowthrough was collected. The flowthrough fractions containing 1,3-β-glucanase were analyzed by trichloroacetic acid (TCA) precipitation and SDS–PAGE analysis. The purified proteins pooled from ten consecutive batches of purification were dialyzed into a solution containing 50 m*M* HEPES pH 8.0 and 50 m*M* NaCl and concentrated to 24 mg ml^{-1}. During the purification process, the enzymatic activity was analyzed by the dinitrosalicylic acid method after mixing protein solution with 0.5%(*w*/*v*) laminarin in 50 m*M* sodium acetate buffer pH 5.5 at 338 K for 5 min (Wood & Bhat, 1988).

2.2. Crystallization and data collection

The vapour-diffusion and microseeding techniques were used to grow 1,3-β-glucanase crystals for data collection. Initial crystallization screens using various concentrations of PEG MME 550–2000, PEG 400–8000 and $(NH_4)_2SO_4$ precipitants and biological buffers identified PEG MME 2000 as a promising precipitant. Further crystallization trials yielded a crystal of 0.5 × 0.5 × 0.5 mm in size that grew in 45% PEG MME 2000, 100 m*M* HEPES pH 7.0, 2 m*M* EDTA, 2 m*M* β-ME and 10 m*M* $CaCl_2$. The crystal took more than five months to grow; it was very hard to reproduce, hard to manipulate and cracked easily despite the good crystal size and diffraction quality. A microseeding technique was employed to reproduce good-quality crystals of suitable size for data collection. A few cracked crystals were harvested, washed with mother liquor and pulverized by vigorous vortexing. After filtering through a 0.2 µm filter membrane, a series of seeding solutions with dilution factors ranging from 10^3 to 10^6 were prepared. Crystallization drops were prepared by mixing 2 µl protein solution at 24 mg ml^{-1} with 2 µl reservoir solution containing 25% PEG MME 2000, 100 m*M* HEPES pH 7.5, 10 m*M* $MgCl_2$ and 0.01% NaN_3. Crystal seeds were then added to the crystallization drop by streaking the droplets with a single hair dipped into the microseeding solution. Droplets were placed on siliconized cover slips and equilibrated against 1 ml reservoir solution at a temperature of 278 K. Reproducible crystals appeared in 3–5 d with optimal dimensions of 0.6 × 0.2 × 0.125 mm. A single crystal

Table 1
Data-collection and refinement statistics.

Values in parentheses are for the highest resolution shell

	Native data	Pt-derivatized data
Space group	$P2_12_12_1$	
Unit-cell parameters (Å)	a = 39.5, b = 76.0, c = 79.7	a = 39.6, b = 76.0, c = 79.8
Resolution range (Å)	20.0–1.5 (1.57–1.50)	20.0–1.5 (1.57–1.50)
Total reflections	167028	158652
Unique reflections	38840	37746
Data redundancy	4.2 (3.4)	4.2 (3.8)
Completeness	99.0 (96.3)	96.0 (97.6)
$I/\sigma(I)$	34.8 (14.4)	31.0 (11.9)
$R_{\rm merge}$† (%)	4.8 (9.8)	4.6 (12.1)
Refinement statistics		
R factor‡ (%)	18.3	
$R_{\rm free}$§ (%)	19.8	
No. of residues	278	
No. of waters	150	
Ramachandran core region¶ (%)	87.2	
R.m.s.d. bond lengths (Å)	0.008	
R.m.s.d bond angles (Å)	1.244	
Average B factor, protein (Å^2)	13.6	
Average B factor, waters (Å^2)	16.5	

† $R_{\rm merge} = \sum_{hkl}\sum_i |I_i(hkl) - \langle I(hkl)\rangle| / \sum_{hkl}\sum_i I_i(hkl)$, where $I_i(hkl)$ is the observed intensity and $\langle I(hkl)\rangle$ is the average intensity of multiple observations of symmetry-related reflections. ‡ $R = \sum |Fp - Fp({\rm calc})| / \sum Fp$. § R factor for a subset of 5% of the reflection data excluded from the structure refinement. ¶ 12.4% of the residues are in additional allowed regions and 0.5% in the disallowed region.

of 1,3-β-glucanase picked up from a droplet in a 0.6 mm diameter mohair loop was transferred into cryoprotectant solution (35% PEG MME 2000, 100 m*M* HEPES pH 7.5, 10 m*M* $MgCl_2$, 0.01% NaN_3) and then placed directly into a cold nitrogen-gas stream at 100 K. The diffraction data were collected on an R-AXIS IV^{++} image-plate system (Rigaku MSC, The Woodlands, Texas, USA). X-rays were generated using a Rigaku RUH3R generator equipped with a copper rotating anode operating at 5.0 kW power rating (50 kV, 100 mA). The X-ray beam was monochromated using Confocal Blue optics and tuned to Cu $K\alpha$ radiation of 1.5418 Å. Data were collected by the standard oscillation method using a crystal-to-detector distance of 80 mm. Images were collected in 0.5° increments with an exposure time of 20 min per image. The data were processed using *HKL* v.1.98 and *SCALEPACK* (Otwinowski & Minor, 1997) and the statistics of the collected data are summarized in Table 1.

2.3. Preparation of derivative crystals

Pt-derivatized crystals were prepared by soaking native crystals in reservoir solutions containing 1–2 m*M* *trans*-$Pt(NH_3)_2Cl_2$ for periods ranging from 4 h to 5 d. Prior to X-ray diffraction screening, the crystals were washed twice with reservoir solution and then transferred to a series of PEG MME 2000 solutions of successively increasing concentration from 25%(*w*/*v*) to 35%(*w*/*v*) in five steps. The crystal was soaked in each PEG MME 2000 solution for 10 min before transferring it to the next solution. For each heavy-atom-soaked crystal, a total of 10° of preliminary X-ray diffraction data were collected with 1.0° oscillation per frame, processed and merged with the native crystal data set using *HKL* v.1.98 and *SCALEPACK* to check high χ^2 values (>10) for isomorphous difference signals. Afterwards, a full data set was collected and the difference Patterson map was calculated using the *CCP*4 program suite for heavy-atom location and phasing (Collaborative Computational Project, Number 4, 1994). Several trials of other derivative crystals soaked with $AgNO_3$, lead(II) acetate or $HgCl_2$ yielded either severe non-isomorphism or poorly substituted derivatives.

2.4. Structure determination and refinement

The 1,3-β-glucanase crystallized in an orthorhombic lattice (space group $P2_12_12_1$), with unit-cell parameters a = 39.5, b = 76.0, c = 79.7 Å. Given the molecular weight of 28 753 Da, the calculated Matthews coefficient ($V_{\rm M}$) was 2.08 Å^3 Da^{-1} and the solvent content was 40.9%. There was one molecule per asymmetric unit. We had previously tried unsuccessfully to use the known crystal structures of 1,3–1,4-β-glucanase from *Bacillus* and *Fibrobacter* and endo-β-galactosidase from *Clostridium* (PDB codes 1byh, 1mve and 1ups) as search models for molecular replacement [the crystal structure of 1,3-β-glucanase from *Nocardiopsis* sp. (Fibriansah *et al.*, 2007) had not then been published]. The current 1,3-β-glucanase crystal structure was determined by single isomorphous replacement with anomalous signal (SIRAS) phasing techniques using the anomalous signal from the platinum derivative at the Cu $K\alpha$ wavelength. The Friedel pairs of the Pt-derivative data were separated while processing and merging the data using the programs *HKL* v.1.98 and *SCALEPACK*. Successive runs of the *SHELXC*/*D*/*E* programs (Sheldrick, 2008) found one major and two minor Pt-atom locations by automatic Patterson interpretation, expanded the anomalously scattering substructure by dual-space direct methods and unambiguously distinguished the heavy-atom enantiomorphs for initial experimental phasing with a map correlation coefficient of 67.5%. The experimentally phased electron-density map was of high quality, enabling 98% of the amino-acid sequence to be automatically traced using *ARP*/*wARP* (Lamzin *et al.*, 2001). The side chains of the automatically traced protein structure were then checked using the molecular-graphics program *O* (Jones *et al.*, 1991). Rigid-body refinement and ten cycles of maximum-likelihood refinement using *REFMAC* 5.0 (Murshudov *et al.*, 1997) were carried out and the calculated composite $2F_o - F_c$ and $F_o - F_c$ maps were examined for misfitted residues or to add missing residues. The composite electron-density map did not show any misfitted residues after ten rounds of refinement with ten cycles each of restrained geometry and isotropic temperature-factor refinement. Water molecules were then added in five rounds of composite difference map generation with calculated σ values of >3.5σ using the program *wARP* (Perrakis *et al.*, 1997). The final model contains 149 water molecules and one Mg atom and has an R factor of 18.3% and an $R_{\rm free}$ of 19.8%. The average atomic B factor for the molecule is

14.4 Å^2. The data-collection and refinement statistics of the final refined molecule geometry are listed in Table 1.

3. Results and discussions

3.1. Overall structure

The structure of the endo-1,3-β-glucanase is shown in Fig. 1. The two C-terminal amino acids (–GL) in the structure were disordered. In addition, we identified that the five amino acids at positions Leu178, His187, Leu190, His222 and Val226 in the electron-density map were actually Ser178, Gln187, Phe190, Gln222 and Ala226, respectively. The nucleotide sequence of the expression vector pUC18 containing the catalytic domain of 1,3-β-glucanase was determined in order to re-confirm the findings in the electron-density map fitting. These changes may arise from sequencing errors in deducing the amino-acid sequence of the entire coding region for 1,3-β-glucanase from an ~3.1 kbp chromosomal DNA (Hong *et al.*, 2002). The overall dimensions of the protein are ~55 × 40 × 34 Å, comprising 18 β-strands, two α-helices and four short 3_{10}-helices based on the *STRIDE* secondary-structure assignment analysis (Frishman & Argos, 1995). The main feature of the protein structure is a core of six- and seven-stranded antiparallel β-sheets in the order β1-β18-β9-β14-β15-β16 and β2-β8-β17-β10-β11-β12-β13 packed against each other to form a β-sandwich jelly-roll motif. The two antiparallel β-sheets are closed off by intertwining connections between the β-strands at the bottom and primarily α-helix H2 at the top. The protein-folding motif is similar to that of 1,3–1,4-β-glucanase from *Bacillus* and the twist and bend of these two β-sheets forms a concave channel on the molecule approximately 15 Å long by 8 Å wide. The top and bottom rim of the concave side are further enveloped by additional protruding loops Phe130–Asn136 and Thr36–Gly48, as well as helix H1 extending from Gly245 to Pro256 to form a channel cleft for glucan binding. The structure has two disulfide bonds at positions Cys161–Cys169 and Cys181–Cys186 connecting β-strands β12–β13 and β13–β14, respectively, which are located on the concave side of the molecule. These disulfide bonds were not observed in the BglF structure (*Nocardiopsis*) and presumably provide structural stability in the local region of the active site. A magnesium ion located close to the N-terminus of the protein is bound in an octahedral geometry to the carbonyl and carboxylate O atoms of Asp16 and Asp269, the carbonyl O atom of Gly66 and a water molecule. It has been suggested that the metal ion is important in stabilizing the protein structure and enzymatic activity of 1,3–1,4-β-glucanase from *Fibrobacter*, which belongs to glycosyl hydrolase family 16 (Tsai *et al.*, 2003).

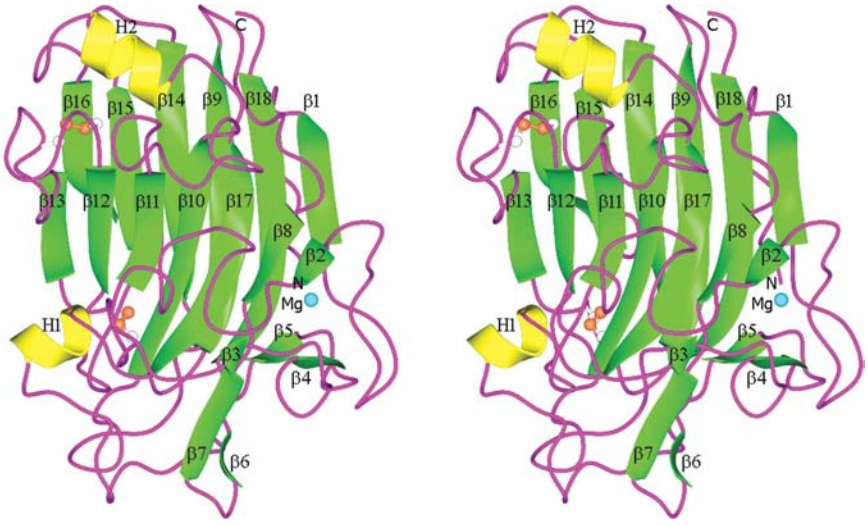

Figure 1
Stereoview of the overall structure of the catalytic domain of 1,3-β-glucanase from *Streptomyces*. The two difulfide bonds are drawn in ball-and-stick representation. The magnesium ion is shown as a cyan sphere. This figure and Figs. 2, 3 and 4 were generated with the program *CCP4mg* (Potterton *et al.*, 2004).

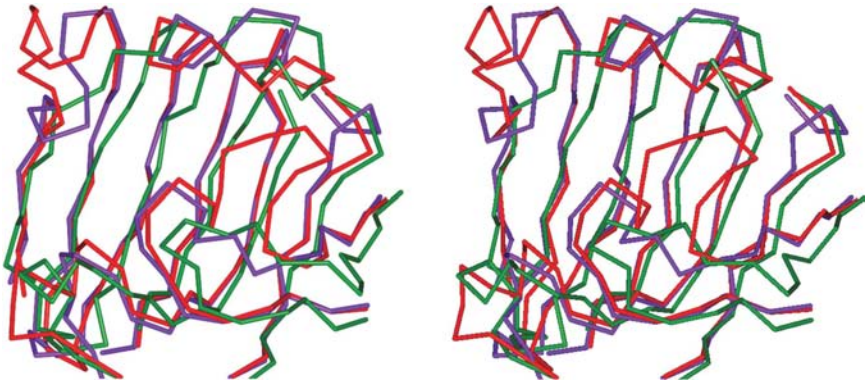

Figure 2
C$^\alpha$-trace backbone superposition of the active cleft for 1,3–1,4-β-glucanase from *Bacillus* (PDB code 1byh; green), 1,3-β-glucanase from *Nocardiopsis* (PDB code 2hyk; purple) and the current structure from *Streptomyces* (red).

3.2. Structure comparison

The crystal structure of 1,3–1,4-β-glucanase from *Bacillus* (PDB code 1byh) and BglF from *Nocardiopsis* (PDB code 2hyk) were used to investigate the structural and sequence variations related to their substrate specificity. BglF shows more than eightfold higher enzymatic activity toward lichinen (1,3–1,4-β-glucan), but also hydrolyzes 1,3-β-glucans such as laminarin, pachyman and curdlan (Masuda *et al.*, 2006). On the other hand, the catalytic domain of the 1,3-β-glucanase from *Streptomyces* preferentially hydrolyzes glucans with 1,3-β-linkages (Hong *et al.*, 2002). Fig. 2 illustrates a structural comparison of the active-site

clefts of these proteins. The residues in the core β-sandwich jelly-roll motif in these homologous proteins are primarily conserved, except that the current structure shows several additional short stretches of residue insertions in the loop regions connecting the β-strands of the β-sandwich motif on the concave side of the molecule. A comparison of the topology of the core motif shows that the best average r.m.s. difference is 2.0 Å for 109 C^{α} atoms between *Streptomyces* 1,3-β-glucanase and *Bacillus* 1,3–1,4-β-glucanase and 0.7 Å for 142 C^{α} atoms between the *Streptomyces* and *Nocardiopsis* 1,3-β-glucanases. A closer examination of the topological variations in the concave active site shows that the average r.m.s. difference is 12.2 Å for 128 C^{α} atoms between *Streptomyces* 1,3-β-glucanase and *Bacillus* 1,3–1,4-β-glucanase and 6.7 Å for 128 C^{α} atoms between the *Streptomyces* and *Nocardiopsis* 1,3-β-glucanases. The sequence similarity between *Streptomyces* 1,3-β-glucanase and BglF is 59% and the similarity between *Streptomyces* 1,3-β-glucanase and *Bacillus* 1,3–1,4-β-glucanase is 39%.

3.3. Substrate-binding and active sites

The concave side of the 1,3-β-glucanase molecule is the active site for β-glucan binding (Fig. 3). A structural difference in the active site between 1,3-β-glucanase and BglF arises from the conformations of three protruding loops connecting the β-strands of the β-sandwich motif and a loop of helix H1. The residues Thr36–Gly48 in loop $\beta2$–$\beta3$ and Phe130–Gly139 in loop $\beta10$–$\beta11$ narrow the width of the cleft to 3 Å based on a calculation using *CAVER* (Petřek *et al.*, 2006). Furthermore, two key residues, Tyr38 and Tyr134, protruding from these two loops, respectively, together with the conserved residues Phe130 and Arg84 on $\beta8$ close the side entrance of the active-site cleft. The closest related active-site cleft with one end closed is that of β-galactosidase from *Clostridium*, which releases the 1,4-α-linked disaccharide GlcNAc-Gal from glucans (Tempel *et al.*, 2005). The GHF16 members with currently known structures, 1,3–1,4-β-glucanase and BglF, both have open-channel active sites. Compared with the $\beta2$–$\beta3$ loop of BglF, that of 1,3-β-glucanase contains an insertion of seven residues (Thr36–Asn44), is glycine-rich and has its flexibility constrained by Pro39 and by hydrogen bonding between the carbonyl O atom of Gly42 and the amide N atom of Gly46. This additional loop does not appear to be flexible with multiple conformations. It provides a protruding residue, Tyr38, for active-cleft closure and the loop itself also provides a non-electrostatic surface that narrows the width of the active-site cleft. All currently known crystal structures of 1,3–1,4-β-glucanases and 1,3-β-glucanases belonging to GHF16 have not shown conformational change upon binding to polysaccharides. Furthermore, the residues Thr163–Ser173 in loop $\beta12$–$\beta13$ and Gly246–Phe252 in loop $\beta17$–$\beta18$ narrow the width of the opening end of the active cleft. A stacking of hydrophobic residues at the bottom rim of the active-site cleft, Trp120 on $\beta10$, Trp156 on $\beta12$, and Phe248 and Phe252 on helix H1, would provide an effective aromatic stacking interaction with the glucopyranose of the substrate. The residues Glu142, Asp144 and Glu147, which are involved in hydrolysis of the 1,3-β-glycosidic bond, are highly conserved in GHF16. Mutations of these residues in BglF abolish the enzymatic activity (Masuda *et al.*, 2006). The one-end closed active-site cleft has a length of ~8 Å, which can only accommodate two glucopyranose units to reach the catalytic residues. A 1,3-β-linked disaccharide was modelled into the active-site cleft by superimposing the β-sandwich

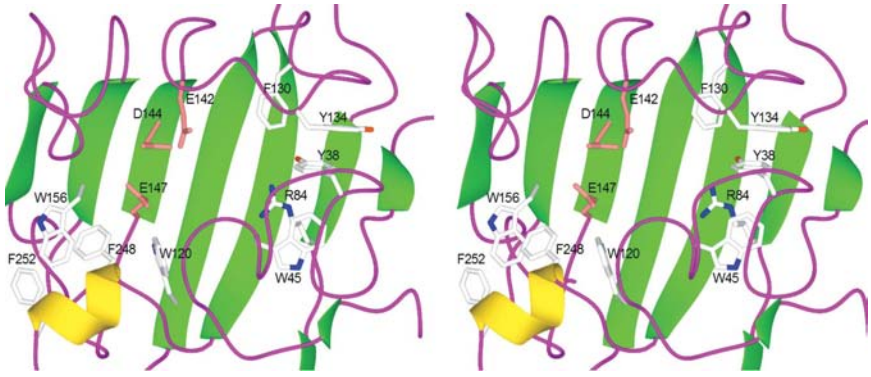

Figure 3
Stereoview of the concave side of the protein's β-sandwich folding motif for β-glucan binding. The β-strands on the back of the motif have been deleted for clarity. Two main residues, Tyr38 and Tyr134, together with the conserved residues Phe130 and Arg84 close the opening of the active-site cleft on the right-hand side. Residues Trp120, Trp156, Phe252 and Phe248 provide a platform for hydrophobic interaction with the glucopyranose ring on the other side of the active-site cleft. The catalytic residues Glu142, Asp144 and Glu147 are shown in pink.

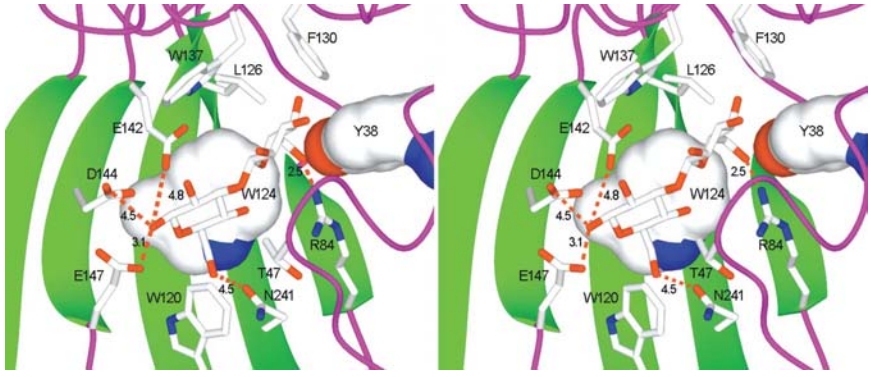

Figure 4
A laminaribiose molecule was modelled into the active-site cleft of 1,3-β-glucanase. The substrate was obtained from the β-glucan tetrasaccharide in complex with a hybrid *Bacillus* 1,3–1,4-β-glucanase (PDB code 1u0a). The model, with minor adjustments using the graphics display program *O*, fits tightly into the active-site cleft without van der Waals steric clashes.

motif of the current structure with the structure of the hybrid *Bacillus* 1,3–1,4-β-glucanase H(A16-M) in complex with β-glucan tetrasaccharide (PDB code 1u0a; Gaiser *et al.*, 2006). The laminaribiose unit (1,3-β-linked disaccharide) of the tetrasaccharide can be fitted into the active-site cleft without van der Waals clashes using the molecular-graphics program *O* (Fig. 4). The cellobiose unit (β-1,4-linkage) could not fit into the active-site cleft very well, as the orientations of the 1,4-β-linked glucopyranose units and the $-CH_2OH$ groups were in the opposite direction to the plane of the disaccharide unit. This result is consistent with the enzyme-activity assay, which showed that 1,3-β-glucan is the most favourable substrate (Hong *et al.*, 2002). The model shows that the interactions of laminaribiose with the active-site residues are mainly hydrophobic. The aromatic ring of Trp137 is within van der Waals contact distance of the glucopyranose unit. Two residues, Thr47 and Leu126, are also within van der Waals contact distance. The C^1-OH group of laminaribose points out towards the bulk-solvent region, which suggests that the leaving direction of one end of the bound long-chain helical 1,3-β-glucan is either curved or bent away from the active-site cleft. The C^1-OH group of the second glucopyranose unit ready for enzymatic hydrolysis is within hydrogen-bonding distance (2.5 Å) of the $O^{\varepsilon 2}$ atom of Glu147. This glucopyranose unit is stacked between two hydrophobic residues, Trp124 and Trp120. Glu147 has been suggested to act as a general acid, protonating the oxygen at the scissile glycosidic bond (Juncosa *et al.*, 1994). Another hydrogen-bonding event is observed between the $N^{\delta 2}$ atom of Arg84 and the O atom of the CH_2OH group, which anchors the glucopyranose unit in the active site. The Glu142 and Asp144 residues interact with each other through hydrogen bonding between the $O^{\varepsilon 2}$ and O^{D1} atoms. Since these two residues are ∼4.5 Å away from the C^1-OH scissile glycosidic bond, it is possible that the putative nucleophilic carboxyl group of Glu142 stabilizes the intermediate by binding to the partially positively charged C^1 atom of the cleaved bond through an ionic interaction. The function of Asp144 is unclear in the current model, although the mutations Asp125Asn in BglF and Asp105Asn in H(A16-M) leave residual activity (Hahn, Olsen *et al.*, 1995; Masuda *et al.*, 2006). Further understanding of the role played by Glu142 and Asp144 would require details of the complex structure with 1,3-β-glucan.

4. Conclusions

The crystal structure of the 1,3-β-glucanase from *S. sioyaensis* provides structural details of the active-site cleft for 1,3-β-glucan-binding specificity. The enzyme has a β-sandwich jelly-roll folding motif very similar to the structures of BglF as well as those of the 1,3–1,4-β-glucanases of hydrolase family 16. However, the active-site cleft is not in an open-channel conformation; instead, the protruding insertion loops connecting the β-strands of the β-sandwich motif provide additional residues, Tyr38 and Tyr134, that close the active-site cleft at one end. The dimensions of the active-site cleft are large enough to allow a laminaribiose unit to reach the catalytic residues. The catalytic centre includes the key residues Glu142, Glu147 and Asp144 for hydrolysis of glycosidic bonds and is highly conserved among these hydrolases. The current structure provides important information on the active-site structure for 1,3-β-glucan-binding specificity and hydrolysis which could be helpful in application for resistance to phytopathogenic fungi.

We are grateful to Dr Y. C. Liaw at the Academia Sinica for help in structure determination. This work was supported by the National Science Foundation through grant NSC90-2113-M-005-032.

References

Chen, C. H., Huang, J. W. & Tzeng, D. S. (2000). *Plant Pathol. Bull.* **9**, 193.
Collaborative Computational Project, Number 4 (1994). *Acta Cryst.* D**50**, 760–763.
Cruz, J. de la, Pintor-Toro, J. A., Benitez, T., Llobell, A. & Romero, L. C. (1995). *J. Bacteriol.* **177**, 6937–6945.
Fibriansah, G., Masuda, S., Koizumi, N., Nakamura, S. & Kumasaka, T. (2007). *Proteins*, **69**, 683–690.
Frishman, D. & Argos, P. (1995). *Proteins*, **23**, 566–579.
Gaiser, O. J., Piotukh, K., Ponnuswamy, M. N., Planas, A., Borriss, R. & Heinemann, U. (2006). *J. Mol. Biol.* **357**, 1211–1225.
Grenier, J., Potvin, C. & Asselin, A. (1993). *Plant Physiol.* **103**, 1277–1283.
Gueguen, Y., Voorhorst, W. G., van der Oost, J. & de Vos, W. M. (1997). *J. Biol. Chem.* **272**, 31258–31264.
Hahn, M., Olsen, O., Politz, O., Borriss, R. & Heinemann, U. (1995). *J. Biol. Chem.* **270**, 3081–3088.
Hahn, M., Pons, J., Planas, A., Querol, E. & Heinemann, U. (1995). *FEBS Lett.* **374**, 221–224.
Henrissat, B. (1991). *Biochem. J.* **208**, 309–316.
Hong, T. Y., Cheng, C. W., Huang, J. W. & Meng, M. H. (2002). *Microbiology*, **148**, 1151–1159.
Jones, T. A., Zou, J.-Y., Cowan, S. W. & Kjeldgaard, M. (1991). *Acta Cryst.* A**47**, 110–119.
Juncosa, M., Pons, J., Dot, T., Querol, E. & Planas, A. (1994). *J. Biol. Chem.* **269**, 14530–14535.
Lamzin, V. S., Perrakis, A. & Wilson, K. S. (2001). *International Tables for Crystallography*, Vol. F, edited by M. G. Rossmann & E. Arnold, pp. 720–722. Dordrecht: Kluwer Academic Publishers.
Masuda, S., Endo, K., Koizumi, N., Hayami, T., Fukazawa, T., Yatsunami, R., Fukui, T. & Nakamura, S. (2006). *Extremophiles*, **10**, 251–255.
Murshudov, G. N., Vagin, A. A. & Dodson, E. J. (1997). *Acta Cryst.* D**53**, 240–255.
Otwinowski, Z. & Minor, W. (1997). *Methods Enzymol.* **276**, 307–326.
Perrakis, A., Sixma, T. K., Wilson, K. S. & Lamzin, V. S. (1997). *Acta Cryst.* D**53**, 448–455.
Petřek, M., Otyepka, M., Banáš, P., Košinová, P., Koča, J. & Damborský, J. (2006). *BMC Bioinformatics*, **7**, 316.
Potterton, L., McNicholas, S., Krissinel, E., Gruber, J., Cowtan, K., Emsley, P., Murshudov, G. N., Cohen, S., Perrakis, A. & Noble, M. (2004). *Acta Cryst.* D**60**, 2288–2294.
Receveur-Brechot, V., Czjzek, M., Barre, A., Roussel, A., Peumans, W. J., Van Damme, E. J. M. & Rouge, P. (2006). *Proteins*, **63**, 235–242.
Selitrennikoff, C. P. (2001). *Appl. Environ. Microbiol.* **67**, 2883–2894.
Sheldrick, G. M. (2008). *Acta Cryst.* A**64**, 112–122.
Tempel, W., Liu, Z.-J., Horanyi, P. S., Deng, L., Lee, D., Newton, M. G., Rose, J. P., Ashida, H., Li, S. C., Li, Y. T. & Wang, B.-C. (2005). *Proteins*, **59**, 141–144.

Tsai, L. C., Shyur, L. F., Lee, S. H., Lin, S. S. & Yuan, H. S. (2003). *J. Mol. Biol.* **330**, 607–620.
Varghese, J. N., Garrett, T. P., Colman, P. M., Chen, L., Hoj, P. B. & Fincher, G. B. (1994). *Proc. Natl Acad. Sci. USA*, **91**, 2785–2789.
Watanabe, T., Kasahara, N., Aida, K. & Tanaka, H. (1992). *J. Bacteriol.* **174**, 186–190.
Wood, T. M. & Bhat, K. M. (1988). *Methods Enzymol.* **160**, 87–112.
Yi, S. Y. & Hwang, B. K. (1997). *Mol. Cell*, **7**, 408–413.